Chapter 6
Localization and Identification of Acoustic and Radio Wave Signals Using Signal Wavefronts with Artificial Intelligence: Applications in Lightning

K. Pirapaharan, P. R. P. Hoole, and S. R. H. Hoole

Abstract Localization of lightning flash occurring at an unknown location may be done by measuring the electromagnetic pulse (LEMP) radiated by the lightning flash, or the sound waves associated with thunder generated by the high current lightning return stroke. Instruments, placed at three locations, measure the sound wave emitted by lightning at an unknown location and localize it. Alternatively, lightning localization may be done by measuring at three or more locations the LEMP radiated by a lightning flash. Such localizers are used, for instance, at airports. We may develop a system to locate a source of sound by studying the possible localization technique used by bats. Bats typically are capable of laryngeal echolocation that enables them to identify their position and move in complete darkness. The bat sound contains a signal with multiple frequency components, as is the case with thunder. Also, the acoustic signal propagation in the atmosphere deviates from a spherical wave propagation due to a number of different factors including absorption of sound in air, non-uniformity of the propagation medium due to meteorological conditions, and interaction with absorbing solid obstacles with acoustic properties that are influenced by the frequency of the acoustic signal. Hence, a test acoustic signal with multiple frequency components is modeled and tested for the application of acoustic signal localization using signal wavefronts. A computer simulation is made to compare the received signal patterns at different distances using the empirical atmospheric attenuation model for acoustic signal attenuation provided in the ISO 9613-2:1996 standard. Further, this chapter also describes a technique for lightning localization using the LEMP measured at three different locations. An appropriate empirical model, similar to the Bruce-Golde model, is proposed for the lightning return stroke current represented by a dipole antenna. The return stroke current proposed, unlike the Bruce-Golde model, is both time and frequency dependent. The return stroke current thus emits multiple frequency components for LEMP radio wave signals. In addition, closed form equations for the signal propagation for the proposed LEMP radio wave field components, in terms of the distance from the origin, are given here. The wavefront of the overall LEMP changes with distance traveled from the lightning flash. The frequency- and distance-dependent LEMP wave shape is used to detect and localize the lightning flash. A computer-coded

© The Author(s), under exclusive license to Springer Nature Switzerland AG 2022

P. Hoole and S. Hoole, *Lightning Engineering: Physics, Computer-based Test-bed, Protection of Ground and Airborne Systems*,
https://doi.org/10.1007/978-3-030-94728-6_6

lightning localizing technique is illustrated to detect the lightning location from the wavefronts of LEMP at different distances from the lightning flash.

6.1 Introduction

An acoustic wave is defined as a phenomenon whereby a transient elastic wave is generated by the rapid release of energy from a localized source. Such is the case when the lightning return stroke releases a large amount of heat energy along the ionized channel of the lightning leader stroke. The process of locating the source of these acoustic waves, by recording the propagating acoustic signals from various sensors and properly analyzing them, is commonly known as the acoustic source localization technique. Kundu (2014) has reviewed the research status of acoustic source localization research technology. Tobias (1976) is a pioneer in the study of acoustic source localization in isotropic materials. The triangulation method proposed by Tobias (1976) is the most commonly used method for isotropic materials. It determines the location of the acoustic source based on the time difference of arrival (TDOA) between the acoustic waves reaching different (a minimum of three) sensors. But only when the precise wave velocity of the elastic wave propagation in the material is obtained, an accurate location result can be obtained. In response to this limitation, the triangulation method has been improved, and an acoustic source localization method suitable for isotropic materials without wave velocity has been proposed by Kundu et al. (2008). However, the localization accuracy of the TDOA method is affected by noise, dispersion effect, energy attenuation, and other factors affecting the wave during the propagation process. The localization accuracy of these methods depends on the measured wave velocity, and the relevant properties of the material need to be obtained in advance. Although the TDOA method is mature and easy to use, its localization accuracy is highly dependent on the accuracy of the measured TDOA.

In this chapter, we propose a new method of localization of acoustic sources for acoustic signals, which contain a range of frequency components. Acoustic energy is dissipated in air by the following two major mechanisms: (a) viscous losses due to friction between air molecules, which results in heat generation and (b) the relaxation processes by which the acoustic energy is momentarily absorbed by the air molecules and causes the molecules to vibrate and rotate. These molecules can then re-radiate sound at a later instant, which can partially interfere with the incoming acoustic signal. Hence, the atmospheric absorption that takes place is a function of frequency, atmospheric properties, and the distance propagated. Thus, the atmospheric absorption coefficient is very dependent on the frequency component of the signal. Moreover, the atmospheric absorption varies for different frequency components at different distances from the acoustic source as per the empirical atmospheric attenuation model for acoustic signal attenuation standard provided in ISO 9613-2:1996. Ultimately, the shape of the received signal variation depends on the

distance traveled. This phenomenon is used to localize the source distance from the receiver location.

A similar technique is used to localize the radio wave signal source since the radio wave propagation amplitude also depends on the frequency components of the current to the dipole antenna model of the return stroke. A current model with different frequency components may be used and the closed form equation for the propagating radio wave field components in terms of the frequency and the distance from the origin is presented. Once again the shape of the radio field components varies, depending on the distance from the origin of the source.

6.2 Methodology: Test Signals and Wavefronts

6.2.1 Methodology for Acoustic Signals

For the novel method of wavefront estimation, the test signal model and the respective wavefront models vary for acoustic and radio wave signals. The wavefront functions for the respective test signal functions are used.

In order to have multiple frequency components, the test signal is selected as follows.

$$S(t) = \sum_{i=1}^{N} A_i e^{-f_i t} \tag{6.1}$$

where A_i, f_i, and N are defined to have $S(t)$ as an energy signal with multiple frequency components. Also, the proposed signal satisfies the condition

$$S(t)|_{t=0} = 0. \tag{6.2}$$

The atmospheric attenuation factor is given as stated in ISO 9613-2:1996. For a standard pressure of one atmosphere, the absorption coefficient α(in dB/m) can be calculated as a function of frequency f (Hz), temperature T (degrees Kelvin), and molar concentration of water vapor h by:

$$\alpha = 8.69 f^2 \left\{ \begin{array}{l} 1.84 \times 10^{-11} (T/T_0)^{1/2} + \\ (T/T_0)^{-5/2} \left[\dfrac{0.01275 e^{-2239.1T}}{F_{r,O} + f^2/F_{r,O}} + \dfrac{0.1068 e^{-3352T}}{F_{r,N} + f^2/F_{r,N}} \right] \end{array} \right\} \tag{6.3}$$

where $T_0\left(293.15^0 K\right)$ is the room temperature in Kelvin while $F_{r,O}$ and $F_{r,N}$ are respective oxygen and nitrogen relaxation frequencies as given below:

$$F_{r,O} = 24 + 4.04 \times 10^4 h \left(\frac{0.02 + h}{0.391 + h} \right) \tag{6.4}$$

$$F_{r,N} = \left(\frac{T}{T_0} \right)^{1/2} \left(9 + 280h\, e^{\left\{ -4.17 \left[\left(\frac{T}{T_0} \right)^{-1/3} - 1 \right] \right\}} \right). \tag{6.5}$$

Thus, the atmospheric attenuation factor A_{atmos} is obtained as:

$$A_{atmos} = e^{-\alpha r} \tag{6.6}$$

where r is the distance over which the wave has been propagated.

Taking the fast Fourier transform (FFT) of $S(t)$ and applying the atmospheric attenuation factor for the respective frequencies and distance traveled, it will yield the FFT of the wavefront at different distances. Finally, by taking inverse FFT, the wavefront is determined at different ranges for the given test signal $S(t)$.

6.2.2 Methodology for Radio Wave Signals

The current to the dipole antenna could be modeled as a sum of exponential terms given below to obtain the current with multiple frequency components:

$$I(t) = \sum_{n=1}^{N} I_n e^{-f_n t} \tag{6.7}$$

where I_n, f_n, and N are defined to give the current signal $I(t)$ as an energy signal with multiple frequency components. Also, the current modeled as such satisfies the following conditions:

$$\left. \begin{aligned} I(t)|_{t=0} &= 0 \\ \left. \frac{dI(t)}{dt} \right|_{t=0} &= 0 \end{aligned} \right\}. \tag{6.8}$$

Selecting the dipole as a vertical dipole of length L, the electrical field components at a distance r could be derived in the spherical coordinate system as:

$$E_r = 2\eta \frac{L \cos\theta}{4\pi} \sum_{n=1}^{N} k_n^2 \left(\frac{1}{(k_n r)^2} + \frac{1}{(k_n r)^3} \right) I_n e^{-f_n t} \tag{6.9}$$

$$E_\theta = \eta \frac{L \sin\theta}{4\pi} \sum_{n=1}^{N} k_n^2 \left(\frac{1}{k_n r} + \frac{1}{(k_n r)^2} + \frac{1}{(k_n r)^3} \right) I_n e^{-f_n t} \tag{6.10}$$

where $k_n = j\sqrt{\mu_0 \varepsilon_0} f_n$ and $\eta = \sqrt{\frac{\mu_0}{\varepsilon_0}}$.

Hence, the resultant electrical field could be expressed as

$$\boldsymbol{E} = E_r \hat{\boldsymbol{r}} + E_\theta \hat{\boldsymbol{\theta}}. \tag{6.11}$$

Thus, the amplitude of the resultant field is

$$|\boldsymbol{E}| = \sqrt{|E_r|^2 + |E_\theta|^2}. \tag{6.12}$$

The resultant electric field is the result of the static charges of the dipole (electrostatic), the DC current in the dipole (magneto-static) and time-varying current in the dipole (radiation). Thus, different contributions predominate the resultant field component at different distances. Consequently, we attempt to use the amplitudes of the resultant field pattern to identify the distance of the source point from the observation point. Thus, the shape and size of the wavefront of the electric (or magnetic) field component could be used to identify the distance from the LEMP source for the empirically modeled lightning current.

We are grateful to Bamunusinghe B.A.A.R. and Dushmantha W.S for the MATLAB^{TM} codes listed below. Moreover, credit for the development of the code in Sect. 5.6.2 is due to Abeywardhana S.A.Y., Senarathne L.R., Subhashini H.A.A. These codes may be used to develop, implement and experiment with the techniques presented in Sects. 5.6.2 and 6.2.

1. Ultrasonic signals: Stationary transmitter

Main function:

```
clear all
clc
%input data
h = 70;%humidity
Fs=400000;%sampling frequncy
%input signal
t=0:1/(2*Fs):(0.0001(1/(Fs)));
y=(23*exp(-2*pi*20000*t)-29*exp(-2*pi*40000*t)+5*exp(-2*pi*60000*t)+1*exp(-
2*pi*80000*t)+23*exp(-2*pi*100000*t)-29*exp(-2*pi*120000*t)+5*exp(-
2*pi*140000*t)+1*exp(-2*pi*160000*t));
B = max(y);
%time domain graph of orginal signal
figure(1)
plot(t,abs(y/B))
xlabel('time(s)');
ylabel('Nomalized values');
title('time domain signal of original')

y1=fft(y);% fast fourier transform of input signal
L2=length(y1);
y2=y1(1:L2/2);
f = Fs*(0:((L2/2)-1))/L2;
A = max(y2);
%frequncy domain graph of orginal signal
figure(2)
plot(f,abs(y2/A))
title('frequency domain singal of original')
xlabel('frequency');
ylabel('Nomalized values');

d=1;%distance between transmiter and object/2
[K] = attenuation_effect(f,h,d,y2,Fs,L2,3);% attenuation fact with graphs
```

Attenuation effect function:

```
function [K] = attenuation_effect(f,h,d,y2,Fs,L2,num)
F_ro = 24 + (40400*h*(0.02+h)/(0.391+h));
F_rn = 9 + (280*h);
A = (6.1425*(10^-6))./(F_ro + (f.^2)/F_ro);
B = (1.0817*(10^-5))./(F_rn + (f.^2)/F_rn);
C = A + B + (1.84*(10^-11));
alpha = C .*(f.^2);
k = exp(-alpha * d);
K = k.*y2;
A = max(K);
%frequency domain graph of attenuated signal
figure(num)
plot(f,abs(K/A));
title(['frequency domain signal when d =',num2str(d)]);
xlabel('frequency');
ylabel('Nomalized values');

t0=(0:2:(L2-2))/Fs;
x = ifft(K);%inverse fourier transform
B = max(x);
%time domain graph of attenuated signal
figure(num+1)
plot(t0,x/B);
title(['time domain signal when d=',num2str(d)]);
xlabel('time(s)');
ylabel('Nomalized values');
end
```

2. Ultrasonic signals: Moving transmitter

Main function:

```
clear all
clc
%input data
Vair=330;   %ultrasonic signal velocity in Air

h = 70;   %humidity
Fs=400000;%sampling frequncy
%input signal
t=0:1/(2*Fs):(0.0001-(1/(2*Fs)));
y=(23*exp(-2*pi*20000*t)-29*exp(-2*pi*40000*t)+5*exp(-2*pi*60000*t)+1*exp(-
2*pi*80000*t)+23*exp(-2*pi*100000*t)-29*exp(-2*pi*120000*t)+5*exp(-
2*pi*140000*t)+1*exp(-2*pi*160000*t));
L=length(y);%length of signal
%time domain graph of orginal signal
figure(1)
plot(t,abs(y))
xlabel('time(s)');
ylabel('Nomalized values');
title('time domain signal of original')

y1=fft(y);% fast fourier transform of input signal
L2=length(y1);
y2=y1(1:L2/2);
f = Fs*(0:((L2/2)-1))/L2;
%frequncy domain graph of orginal signal
figure(2)
plot(f,abs(y2))
title('frequency domain singal of original')
xlabel('frequency');
ylabel('Nomalized values');

Vobject=100;%object velocity
d=1;
%doppler shift
t0 = doppler_shift(Vair,Vobject,1/Fs);

%doppler shifted signals
Fs_new = 1/t0;
f = Fs_new*(0:((L2/2)-1))/L2;
t=0:1/(2*Fs_new):((L-1)/(2*Fs_new));
num=3;
[K] = attenuation_effect(f,h,d,Vobject,y2,Fs_new,L2,num);
```

Attenuation effect function:

```
function [K] = attenuation_effect(f,h,d,Vobject,y2,Fs,L2,num)
F_ro = 24 + (40400*h*(0.02+h)/(0.391+h));
F_rn = 9 + (280*h);
A = (6.1425*(10^-6))./(F_ro + (f.^2)/F_ro);
B = (1.0817*(10^-5))./(F_rn + (f.^2)/F_rn);
C = A + B + (1.84*(10^-11));
alpha = C .*(f.^2);
k = exp(-alpha * d);
K = k.*y2;
A = max(K);
%frequency domain graph of attenuated signal
figure(num)
plot(f,abs(K/A));
title(['frequency domain signal when d,Velocity =',num2str(d),',',num2str(Vobject)]);
xlabel('frequency');
ylabel('Nomalized values');

t0=(0:2:(L2-2))/Fs;
x = ifft(K);%inverse fourier transform
B = max(x);
%time domain graph of attenuated signal
figure(num+1)
plot(t0,x/B);
title(['time domain signal when d,Velocity =',num2str(d),',',num2str(Vobject)])
xlabel('time(s)');
ylabel('Nomalized values');
end
```

Doppler function:

```
function [t0] = doppler_shift(Vair,Vobject,Ts)
if  Vobject>0
   t0=Ts*(Vair-Vobject)/(Vair+Vobject);
else
   t0=Ts*(Vair+abs(Vobject))/(Vair-abs(Vobject));
end
end
```

3. Microwave signals

```
Main function:

clear all
clc
Fs=8000000000;%sampling frequncy
%input signal
angle1 = 0.00000002;
angle = pi/6;
t=0:1/(10*Fs):(0.00000001-(1/(Fs)));
y=(23*ex p(-2*pi*250000000*t)-29*exp(-2*pi*300000000*t)+5*exp(-
2*pi*400000000*t)+1*exp(-2*pi*950000000*t));

A1=23000;
A2=-29000;
A3=5000;
A4=1000;
f1=250000000;
f2=300000000;
f3=400000000;
f4=950000000;
k1=250000000j*(2*pi*3.4*(10^-9));
k2=300000000j*(2*pi*3.4*(10^-9));
k3=400000000j*(2*pi*3.4*(10^-9));
k4=950000000j*(2*pi*3.4*(10^-9));
r=2;
E_r = 2*cos(angle)*(((k1^2)*A1*exp(-
2*pi*f1.*t)*((1/(k1*r)^2)+(1/(k1*r)^3)))+((k2^2)*A2*exp(-
2*pi*f2.*t)*((1/(k2*r)^2)+(1/(k2*r)^3)))+((k3^2)*A3*exp(-
2*pi*f3.*t)*((1/(k3*r)^2)+(1/(k3*r)^3)))+((k4^2)*A4*exp(-
2*pi*f4.*t)*((1/(k4*r)^2)+(1/(k4*r)^3))));
E_t = sin(angle)*(((k1^2)*A1*exp(-
2*pi*f1.*t)*((1/(k1*r)^2)+(1/(k1*r)^3)+(1/(k1*r))))+((k2^2)*A2*exp(-
2*pi*f2.*t)*((1/(k2*r)^2)+(1/(k2*r)^3)+(1/(k2*r))))+((k3^2)*A3*exp(-
2*pi*f3.*t)*((1/(k3*r)^2)+(1/(k3*r)^3)+(1/(k3*r))))+((k4^2)*A4*exp(-
2*pi*f4.*t)*((1/(k4*r)^2)+(1/(k4*r)^3)+(1/(k4*r)))));

E = ((abs(E_r).^2)+(abs(E_t).^2)).^(0.5);

figure(1)
plot(t,abs(E))
xlabel('time(s)');
ylabel('Electrical field(E)');
title("Time domain signal when r=2");
```

6.3 Test Results

6.3.1 Test Results of Acoustic Signal Model

The test results are simulated for the acoustic model and the radio wave model of LEMP. The results have proven that the two model-based signal processing approaches could be utilized for the localization of the signal source point.

Table 6.1 Parameters of the acoustic signal in the basic model Eq. (6.1).

i	A_i	f_i
1	23	4000 π
2	−29	8000 π
3	5	12000 π
4	1	16000 π
5	23	20000 π
6	−29	24000 π
7	5	28000 π
8	1	32000 π

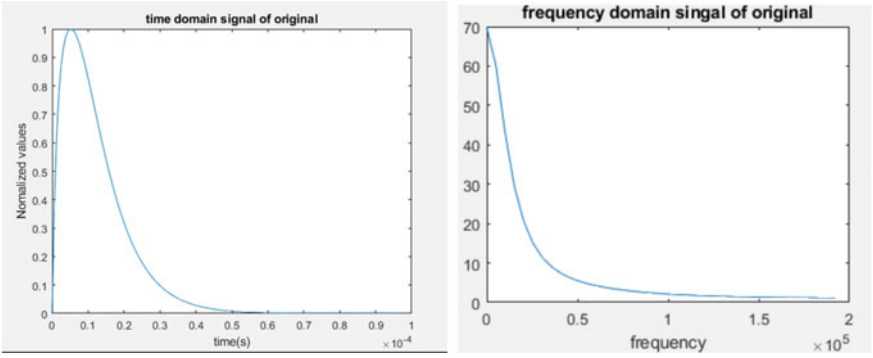

Fig. 6.1 Time and frequency domain pattern at the origin

The test signal is modeled as given in (6.1) by satisfying the conditions given in (6.2). A_i, f_i, and N values are selected as in Table 6.1.

The basic acoustic signal parameters are selected as given in Table 6.1, and the FFT of the signal is obtained. The atmospheric attenuation factor obtained in (6.6) is used in the FFT terms of the signal, and the multiple frequency component signal output of the FFT at different distances is combined to get the resultant signal in the frequency domain. Finally, the inverse FFT is obtained to get the time domain wavefront of the signal at different distances. The wavefront patterns at different distances are shown in Figs. 6.1, 6.2, 6.3, 6.4 and 6.5.

The results in Figs. 6.1, 6.2, 6.3, 6.4 and 6.5 show distinct changes of field patterns with respect to the distance from the source. Therefore, this change of field pattern characteristics could be used to localize the source location from the observation points.

6.3.2 Test Results of Radio Wave Model

The empirical model of the lightning current is as given in (6.7), with the conditions given in (6.8) satisfied. I_n, f_n, and N values are selected as in Table 6.2.

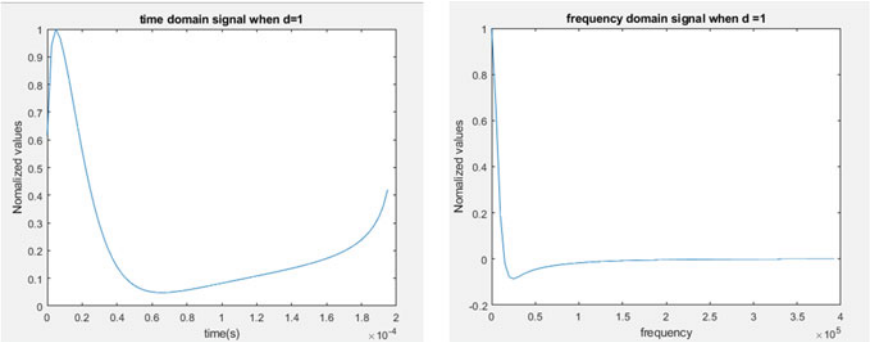

Fig. 6.2 Time and frequency domain pattern at 1 m from the source

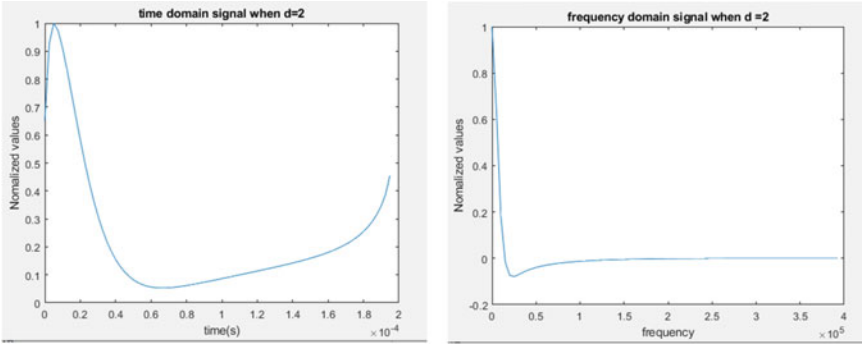

Fig. 6.3 Time and frequency domain pattern at 2 m from the source

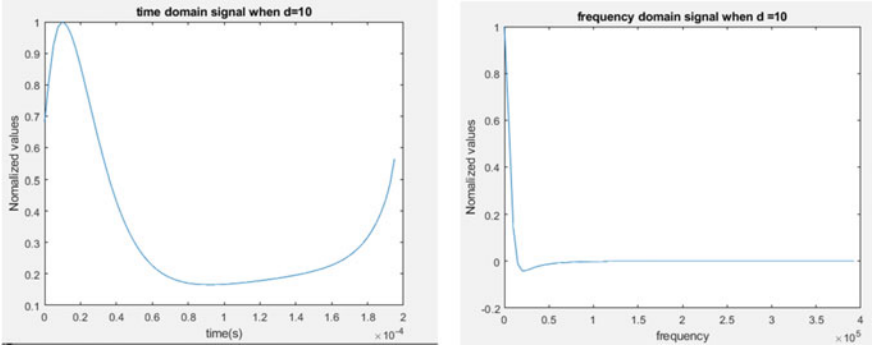

Fig. 6.4 Time and frequency domain pattern at 10 m from the source

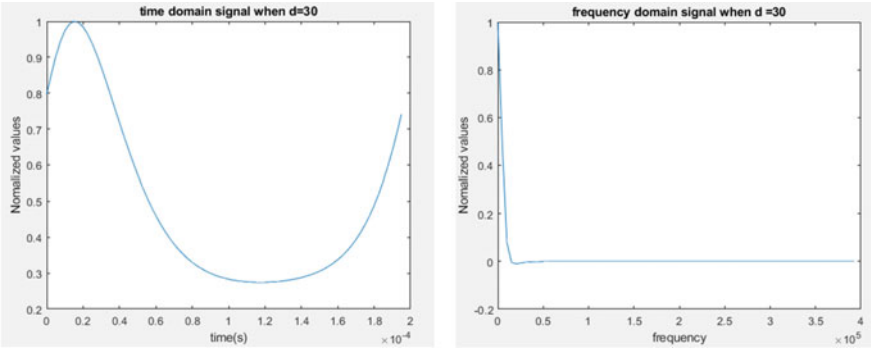

Fig. 6.5 Time and frequency domain pattern at 50 m from the source

Table 6.2 Parameters of the current in the basic model

n $N = 4$	I_n	f_n	Time Constant $\tau_n = \frac{1}{f_n}$ μs
1	-29×103	3×10^6	0.333
2	23×103	2.5×10^6	0.400
3	5×103	6×10^6	0.167
4	1×103	9.5×10^6	0.105

The basic return stroke current signal model parameters are selected as given in Table 6.2. The wavefront of the electrical field signal patterns is calculated using the governing Eqs. (6.9)–(6.12) derived for the current signal defined in (6.7). The return stroke current pattern is shown in Fig. 6.6. The LEMP electrical field wavefront patterns are shown in Figs. 6.7, 6.8, 6.9, 6.10 and 6.11 for a range of distances from 2 m to 10 km from the lightning flash. Only the magnitudes are plotted in Figs. 6.7, 6.8, 6.9, 6.10 and 6.11.

Fig. 6.6 Current Signal Pattern

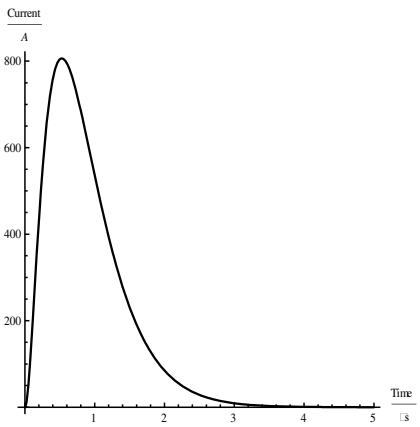

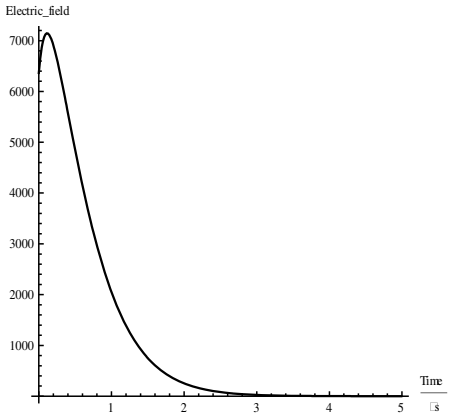

Fig. 6.7 Electrical field at 10 m

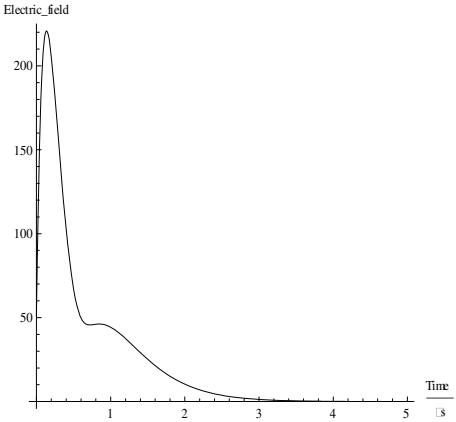

Fig. 6.8 Electrical field at 50 m

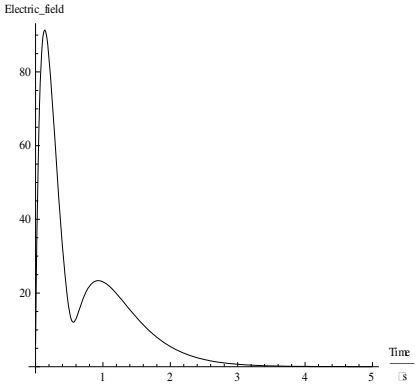

Fig. 6.9 Electrical field at 100 m

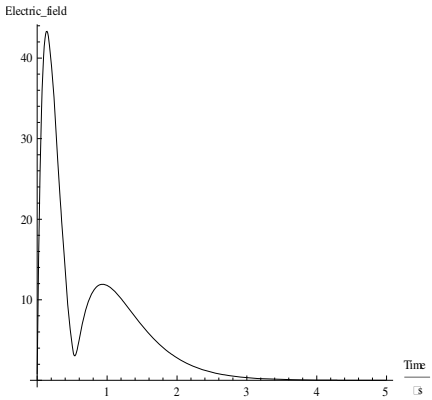

Fig. 6.10 Electrical field at 200 m

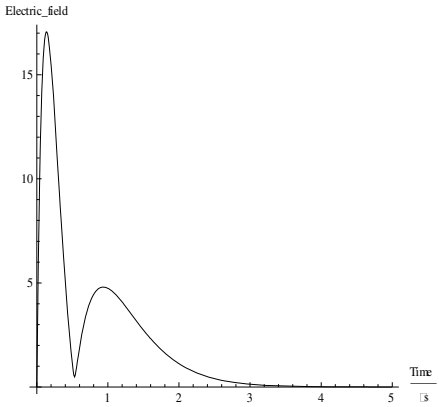

Fig. 6.11 Electrical field at 500 m

The radiated electric field results of Figs. 6.7, 6.8, 6.9, 6.10, and 6.11 show distinct changes in time-domain electric field patterns depending on the distance from the current source (Fig. 6.6), that is, the point of lightning flash. Therefore, this difference in electric field pattern characteristics could be used to localize the source with respect to the observation points where the time-domain electric fields are measured.

6.4 An Array Antenna for Direction and Identity of Lightning Radiated Signals

We have presented in the above sections how lightning may be localized by using both the LEMP and acoustic signals from a lightning flash. However, two issues have not been addressed in the above sections. These are:

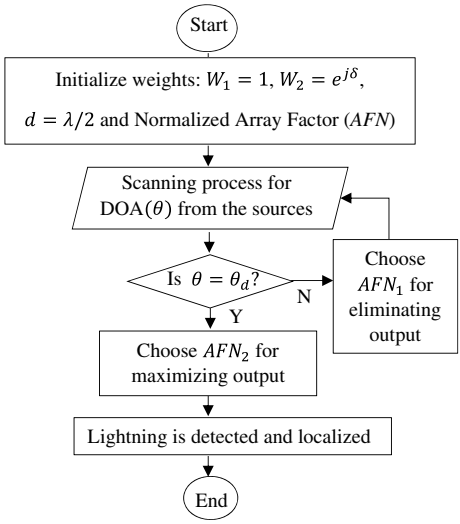

Fig. 6.12 The flowchart of the simultaneous scan Adapted from Singkang et al. (2021) courtesy of The Electromagnetics Academy

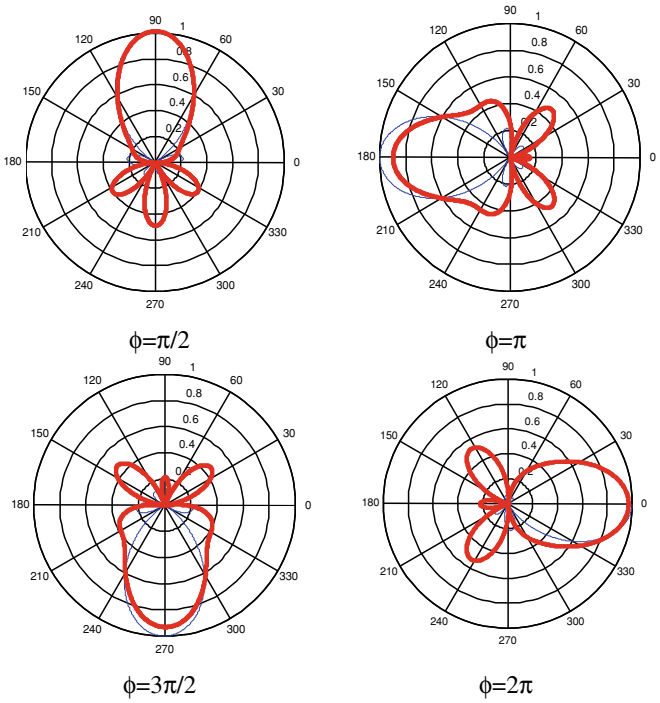

Fig. 6.13 ANN-driven rotating smart antenna beam (from Hoole 2020)

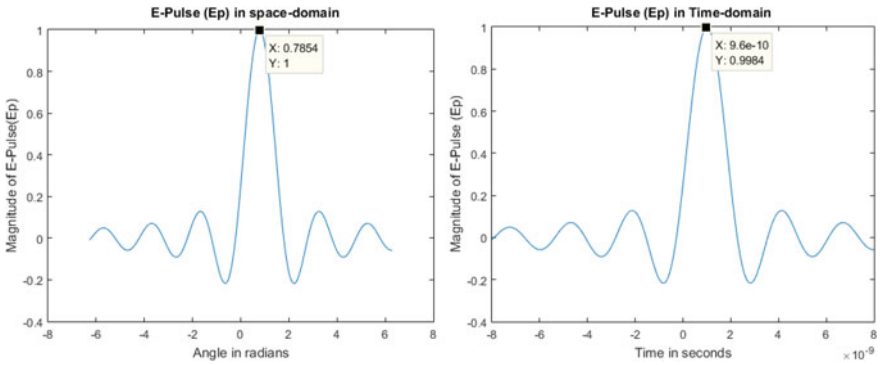

Fig. 6.14 The waveforms of *maximum electric field* generated at 125 MHz (Singkang et al. (2021) reproduced courtesy of The Electromagnetics Academy)

1. Having determined the distance of the lightning flash from the point at which the signal has been measured, how do we know from which specific direction the signal came? In communication systems, this is called the Angle of Arrival (AoA) and is extensively described in Hoole (2020). Here, we shall outline the basic technique to determine the direction from which the lightning impulse has arrived at the observation or measurement point. More specifically, we shall outline the use of an Artificial Neural Network driven smart antenna technique to determine the direction from which the LEMP arrives. The same technique, with acoustic sensors, may be used to detect the direction from which the acoustic signal, associated with thunder, arrives.
2. How do we know that the signal captured is from lightning, and is not from another source, such as a nuclear explosion radiating nuclear electrometric pulse (NEMP) or acoustic sound from a gunshot or bomb explosion? The technique we outline here is based on recognizing the waveform of a signal specifically from lightning. The applications of these techniques are manifold, for instance, identifying gunfire in a mass social gathering where there are firecrackers being lit.

Consider a steerable beam, two-element array antenna being used to measure the LEMP. For a two-element array antenna in receiving mode with one of the two elements containing a digital beam steering (beamforming) weight (w), our task is to scan the region around the lightning area or in a smart city with smart antennas, in the plane that is parallel to the earth surface. The total output from the two-element array antenna is given by

$$E_T = w_1 E_1 + w_2 E_2 \tag{6.13}$$

where E_1 and E_2 are the electric fields picked up by the two antenna elements, with the received signal of the second element multiplied by the electronic weight, w. For a lightning flash occurring at a distance *R* from the apparatus, and at an azimuth

angle θ, the dipoles pick up electric fields of

$$E_1 = \mu_0 \, j\eta \frac{kIh}{4\pi R} \, e^{-jkR} \sin\theta \tag{6.14}$$

$$E_2 = \mu_{0\theta} \, j\eta \frac{kIh}{4\pi R} \, e^{-jkR} \sin\theta \left(e^{jkd \sin\theta \cos\varphi}\right); \tag{6.15}$$

where η is the free space intrinsic impedance; h is the length of the antenna (for half-wavelength dipole, $h = \lambda/2$, and wave number $k = 2\pi/\lambda$) and I is the current flowing along with the lightning flash. Therefore, the total electric field picked up by the array antenna is as defined in (6.13) where the weights w_1 and w_2 are determined by the Perceptron (a single-layer artificial neural network), which being trained based on the specific location of each apparatus, we must cyclically keep under observation. The rotating antenna beam captures the maximum LEMP in the direction of $\theta = \theta_d$ and $\varphi = \varphi_d$ where the angles (θ_d, φ_d) indicate the direction of the lightning flash. The best moment of capturing the lightning flash activity is when the antenna beam is pointed directly towards the location where the lightning flash is generated, when$AF_m = 2$. Since the LEMP has the rise times of the order of a sub-nanosecond (1 GHz) to microsecond (1 MHz), the sampling frequency of the signals received by the array antenna will be in the microwave spectrum for nanosecond radiation from the lightning flash. For the antenna beam to enable the sampling of received signals at every 30° (the segment angle used in fourth-generation wireless communication systems), the microprocessor (depending on the clock frequency) should change the w_1, w_2 values to ensure that the beam rotates, searching for the lightning flash and sample LEMP at 2 GHz. One further step is to use a single beam smart antenna instead of two symmetrical beams generated by the linear array antenna because two symmetrical beams require a reflector to fold one of the beams over. Thus, we can use the non-linear three-element smart antenna, which is capable of generating a single, steerable beam, as described in Hoole (2020).

6.5 Application of the Perceptron ANN for UHF Lightning Flash Detection

An ANN is a numerical structure, which comprises of interconnected artificial neurons, on a substantially littler scale, and works like that of a natural neural system or brain. An ANN can gain from information either in a managed or unsupervised way and can be utilized as a part of assignments, for example, arrangement, relapse, grouping, and many more from there. The human brain gets signals from sensors, for example, the eye, ear, and touch. These signals are then processed by the brain. In ANN, the sensors might be genuine image sensors (camera), sound sensors (microphone), or capacitive touch sensors, which are the inputs to the ANN. Figure 6.16 simplifies the concept of applying the Perceptron ANN training algorithm for UHF lightning flash LEMP angle of arrival (DoA) Detection based on a two-element array

antenna to form the smart antenna (Hoole 2020). On account of the Smart Model-Based Testing as proposed in Singang (2021), the inputs are normally transmitted signals from transmitting antennas. The input signals are processed mathematically, for example by multiplying each input signal by a number (weight, w) and phase-shifting the signal (complex weights, b), at that point sum up the input signals and place it at the output as a transfer function that will yield the final output signals. On account of the human brain, the final output signals might be activating signals to the muscles, for example, to move the human body for activity. In Fig. 6.12, the use of an ANN-driven smart antenna where the beam is rotated and the direction of arrival DOA) of a lightning LEMP is detected.

For the smart antennas, the final output signals might be to divert the beamforming towards the desired users. An ANN is structured of a substantial number of highly interconnected processing elements called artificial neurons organized in layers. The weights (w) and biases (b) are known as adjustable scalar parameters (also known as hyperparameters) of the neuron. The parameters can be adjusted to meet the desired behavior as part of the network training process. An ANN is preferable in many applications as it was fast convergence and adaptive to any complex changes. The hyperparameters (i.e. the parameters used to control the learning process), the learning rate (step size) and the bias of the perceptron control the values of weights calculated and the convergence rate of the perceptron. Therefore, selecting the initial values for these hyperparameters is crucial. However, this Perceptron ANN algorithm has some limitations. These include some series of sufficient trainings to obtain the optimum perceptron hyperparameters if one needed to apply more than the two-element array antenna to meet the desired behavior. This algorithm is designed to detect, localize, and identify the EMP but not to classify the EMP signal. The Perceptron ANN was incorporated with a linear array antenna to form a smart antenna. The linear structure of the array antenna was used due to its low complexity and it can perform beamforming in a single plane within the angular sector. This smart antenna can simultaneously scan and detect any abnormal electrical discharge activity such as the lightning flashes, using the Direction of Angle (DOA) of the LEMP from the lightning flash. Two conditions were considered in this investigation, i.e. to eliminate the interferer signals (signal from an undesired direction) and to maximize the desired signal (from the desired direction).

The Electromagnetic Pulse (*EP*) is used in representing the LEMP for simulation purposes. The radiation pattern of the desired output LEMP signals of Figs. 6.7, 6.8, 6.9, 6.10, 6.11, 6.12, 6.13 and 6.14 may be detected by a time-domain frame that is represented by a *sinc* function in the time-domain. The beam is steered by a Perceptron ANN trained to different locations by another spatial-domain using a *sinc* function. The spatial radiation pattern of the desired output signals traversing in different directions, defined is by $y_d = sinc(\varphi - \varphi_m)$. For a series of DOA (directions of signal arrival), randomly selected at $\varphi_m = 45°, 120°$, and$300°$ there will be a unique time delay of DOAs due to the small differences in the distances between the transmitter and the observation points at which the signals are observed (Hoole, 2020). The similarity of the desired output waveforms in space and time-domain makes the technique efficient, demanding minimal computational complexity. This similarity shows the same ANN used in Smart Antenna (SA) spatial-beam optimization and *e*lectric field detection. In Fig. 6.17, the smart antenna single beam is shown

being rotated by the Perceptron ANN over any desired direction around the observation point. The antenna beam may be cyclically rotated by pre-trained weights to detect and to identify lightning activities, as also the case with electrostatic discharges inside a power substation. As observed, the beam is being focused in the specified DOA.

Figure 6.13 shows the Perceptron ANN-generated beam, focused towards the spatial location of 45° and the simultaneous time-domain search to match the received signal with the time-domain pulse for LEMP detection. The waveforms showed that there is a similarity of the waveforms in space-domain (the beam pointing towards a power apparatus at 45°) and time-domain (a UHF lightning flash current generated LEMP). The maximum peak of *electric field* in space-domain denoted as $\theta_{m,}$ representing the delay angle of DOA. Details of complex methods for electric signal source localization may be found in Hoole (2020).

Figure 6.14 shows the spatial antenna beam and time-domain pulse picked up in the band encompassing 125 MHz at DOA = 45°. In the space-domain of the antenna beam, the maximum magnitude, y = 1 observed at an angle of 0.7854 rad, while in time-domain pulse, the peak magnitude, y = 0.9984 showed peak time, $t_p = 9.6e^{-10}s$. Thus, at the peak time of 0.96 ns, the frequency allowed into the antenna receiver is 1.04 GHz. As observed, for the 1 ns peak LEMP, the error is 4%. Therefore, the accuracy for LEMP signal detection and localization is about 96%.

Following are the MATLABTM computer codes used for ANN training and beam forming:

(Main)

```
%% Program to predict the antenna output
clear;
clc;

%% Data Generation
angle = 0:0.1:2*pi;
Xin = [exp(1i*pi*cos(angle))' ones(size(angle,2),1) exp(-
1i*pi*cos(angle)')];
Yd = cos(2*angle)';

%% Network Training
learningRate = 0.9;
maxEpoch = 1000;
C = spso_train(Xin,Yd,learningRate,maxEpoch);
disp('Trained weights with bias = ');
disp(C);

%% Network Test
out = spso_classify(C,Xin);
error = abs(sum(sqrt((out-Yd).^2)));      % Total squared error
disp(['Error = ' num2str(error)]);
```

Training

```
function C = spso_train(data,labels,alpha,maxEpoch)
%
% Initialize all the variables
[n,m] = size(data);
O = 1;       % Single output
W = randn(m+1,O);        % Random initial weights with bias
W = max(min(W,0.5),-0.5);        % Limit weights to -0.5 until 0.5
%
% Training phase
for epoch = 1:maxEpoch    % Loop until max epoch is reached
    error = 0;  % Initialize error to 0

    for k = 1:n  % Present each and every data
        x = horzcat(1,data(k,:));    % Load the current data as x and
add bias signal
        y = x * W;  % Claculate the output

        % Activation function  (sigmoidal)
        y = (1/(1+exp(-y)));

        % If error occured, update the weights
        if y ~= labels(k)
            error = error + (labels(k) - y);
            W = W + alpha * labels(k) * transpose(x);
        end
    end

    % If no error occured during this epoch, exit
    if error < 0.1
        break;
    end
end
%
% Return the final weight values
C = W;
```

RMSError

```
%% Simple_Perceptron_Single_Output
%-------------------------------------------------------------------------
----%
function labels = spso_classify(C,data)
%
% Initialize all the variables
[n,~] = size(data);
y = zeros(n,1);

for k=1:n  % Present each and every data
    x = horzcat(1,data(k,:));   % Load the current data as x and add
bias signal
    y(k) = x * C;   % Calculate the output y

    % Activation function (bipolar sigmoidal)
    y(k) = (1/(1+exp(-y(k))));

end
%
% Return the labeled output
labels = y;
%-------------------------------------------------------------------------
----
```

For further details on rotating beam antennas for sensing, the reader may consult Hoole (2020).

6.6 Conclusion

Lightning energy signal models covering a range of frequencies are proposed as the source signal for lightning radiated acoustic (thunder) and radio wave signal (LEMP)-based source localization. The governing equations for the propagation of acoustic and radio wave signals for the proposed signal models are based on the respective general equations of acoustic and radio wave propagations. Having simulated the proposed model signal for the governing equations, distinct changes of received signals for different distances from the source were observed. It was shown that the received lightning generated acoustic and radio wave (LEMP) signals can be used to localize the signal source (i.e. the lightning strike point return stroke current) using the the signal models and source localization techniques proposed.

Bibliography

Ahadi, M., Bakhtiar, M.S.: Leak detection in water-filled plastic pipes through the application of tuned wavelet transforms to acoustic emission signals. Appl. Acoust. **2010**(71), 634–639 (2010)
Golde, R.H. (ed.): Lightning, vol 1: Physics of Lightning, Academic Press (1977)

Hoole, P.R.P.: Smart Antennas and Electromagnetic Signal processing for Advanced Wireless Technology: with Artificial Intelligence and Codes. River Publisher (2020)

Hoole, P.R.P; Pirapaharan, K; Kavi, M; Fisher. J; Nur Farah Aziz; Hoole, S.R.H..: Intelligent localisation of signals using the signal wavefronts: A Review. In: International Conference on Lightening Protection(ICLP), Shankai, China (2014)

ISO 9613-2:1996 (en): Attenuation of sound during propagation outdoors-Part 2: General method of calculation (1977)

Kundu, T., Das, S., Martin, S.A., Jata, K.V.: Locating point of impact in anisotropic fibre reinforced composite plates. Ultrasonics **2008**(48), 193–201 (2008)

Kundu, T.: Acoustic source localization. Ultrasonics **54**, 25–38 (2014)

Kunsei, H., Pirapaharan, K., Hoole, P.R.P.: A new fast, memory efficient wireless electromagnetic beamformer antenna with fast tracking for 5/6G systems. Progress in Electromagnetics Research PIER B (2021)

Kunsei, H., Pirapaharan, K. Hoole, P.R.P. Hoole, S.R.H.: Tracking Everyone and everything in smart cities with an ANN driven smart antenna. In: Jude Hemanth D. (ed.) Mobile Learning techniques for Smart City Applications: Trends and Solutions. Springer Nature (2021)

Pirapaharan, K., Kunsei, H., Senthilkumar, K., Hoole, P. R. P., Hoole, S.R.H.: A single beam smart antenna for wireless communication in a highly reflective and narrow environment. In: International Symposium on Fundamentals Electrical Engineering, pp. 1–5 (2016)

Senthilkumar, K.S., Pirapaharan, K., Hoole, P.R.P., Hoole, S.R.H.: Single perceptron model for smart beam forming in array antennas. Int. J. Electric. Comput. Eng. **6**(5), 2300 (2016)

Singkang, L.M.B., Ping, K.A.H., Hoole, P.R.P.: Electric discharges localization for substation fault monitoring using two elements sensor. J. Comput. Theor. Nanosci. **17**(2–3), 1009–1013 (2020)

Singkang, L.M., Ping, K.A.H., Kunsei, H., Senthilkumar, K., Pirapaharan, K., Haidar, A.M., Hoole, P.R.P.: Model based-testing of spatial and time domain artificial intelligence smart antenna for ultra-high frequency electric discharge detection in digital power substations, vol. 99, PIER, pp. 91–101 (2021). https://doi.org/10.2528/PIERM20090301. http://www.jpier.org/PIER/, (CHECK LAS AND FIRST NAMES HERE, 2021)

Tobias, A.: Acoustic-emission source location in two dimensions by an array of three sensors. Non-Destr. Test **9**, 9–12 (1976)